PREDICTION OF HIGH-ALPHA VEHICLE DYNAMICS#

Lars E. Ericsson

Lockheed Missiles & Space Company, Inc.
Sunnyvale, California, USA

ABSTRACT

The long slender nose of an advanced fighter aircraft, maneuvering at high angles of attack, experiences flow separations of various types, which not only generate large local aerodynamic forces but also can generate large downstream loads through the interaction by the shed vortices with wing and tail surfaces. The separation-induced local side force can exceed the local normal force and result in yawing moments well beyond the control capability of existing aircraft. The coupling between vehicle motion and forebody flow separation causes self-induced coning and nose-slice motions. Additionally, the interaction between separation-induced forebody vortices and downstream lifting surfaces can produce dynamic stability problems, resulting in excessive wing rock oscillations, as has been demonstrated in subscale wind tunnel and flight tests. The fluid dynamic processes causing these dynamic stability problems are described and a step-by-step process is outlined for the development of needed predictive capabilities.

LIST OF SYMBOLS

b	wing span
c	reference length, mean chord for wing-body, maximum diameter (d) for body alone
d	cylinder diameter
ℓ	sectional lift, coefficient $c_\ell = \ell'/(\rho_\infty U_\infty^2/2)\, c$
ℓ	rolling moment: coefficient $C_\ell = \ell/(\rho_\infty U_\infty^2/2)Sb$
n	yawing moment, coefficient $C_n = n/(\rho_\infty U_\infty^2/2)Sb$
p	roll rate
Re	Reynolds number based on d_{max} and freestream conditions; usually $Re = U_\infty d/\nu_\infty$
r	yawing rate
S	reference area, $S = \pi d^2/4$ for body alone, S = projected wing area for aircraft
t	time
U_w	wall velocity
U_∞	freestream velocity
Y	side force, coefficient $C_Y = Y/(\rho_\infty U_\infty^2/2)S$
α	angle of attack
β	sideslip angle
ρ	air density
ϕ	roll angle
ψ	coning angle
ν	kinematic viscosity

This paper is based upon results developed under contract to Flight Dynamics, Lab/FIGC, Wright Patterson AFB, Contract No. F33615-87-C-3607, monitored by W. B. Blake.

SUBSCRIPTS

W wall

wr wing rock

∞ freestream conditions

DIFFERENTIAL SYMBOLS

$\dot{\psi} = \partial\psi/\partial t$

$C_{nr} = \partial C_n/\partial(\frac{br}{2U_\infty})$; $C_{n\dot{\beta}} = \partial C_n/\partial(\frac{b\dot{\beta}}{2U_\infty})$

I. INTRODUCTION

Present day high performance aerospace vehicles are subject to unsteady flow fields which generate highly nonlinear aerodynamics with strong coupling between longitudinal and lateral degrees of freedom.[1-3] The complex vehicle dynamics are caused by separated flow effects of various types and can, therefore, usually not be predicted by theoretical means. As a consequence, heavy reliance has to be placed upon phenomenological analyses, based on classic fluid mechanics and guided by flight data and dynamic subscale tests,[4] where dynamic support interference[5,6] and dynamic simulation problems[7,8] add to the difficulty of determining the fullscale separated flow characteristics. Experimental results for high performance aircraft are analyzed to obtain the understanding of the flow phenomena needed for prediction of such aircraft motions as nose-slice and wing rock.

II. DISCUSSION

The results[9] in Figure 1 illustrate some aspects of the problem facing the vehicle designer. First, the yawing moment at $\alpha > 40°$ exceeds greatly the available control capability and, secondly, static test results can be highly confusing. It is somewhat of a relief to find that the huge yawing moments in Figure 1 are almost entirely caused by the loads generated on the slender forebody (at zero side-slip) by asymmetric flow separation, as has been demonstrated for a generic aircraft model in static tests[10] and an advanced aircraft model in dynamic tests[11] (Figure 2). Thus, body-alone aerodynamic results will represent the high-alpha yaw characterics of the complete aircraft. As will be shown, the high-alpha roll characteristics are also to a large extent determined by the aerodynamic characteristics of the slender aircraft forebody.

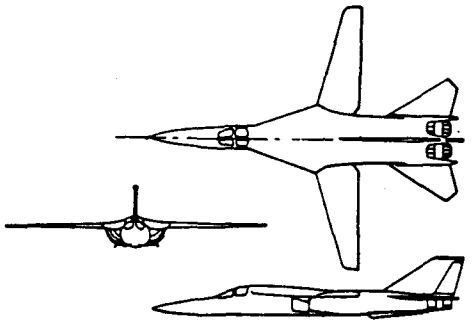

THREE-VIEW SKETCH OF CONFIGURATION WITH LONG POINTED NOSE

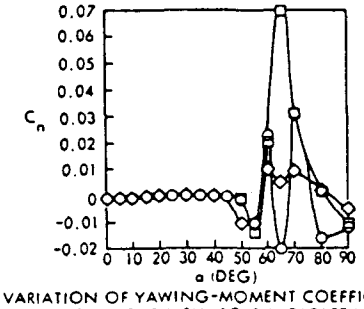

a. VARIATION OF YAWING-MOMENT COEFFICIENT WITH ANGLE-OF-ATTACK, SYMBOLS INDICATE VALUES OBTAINED IN SEVERAL REPEAT TESTS

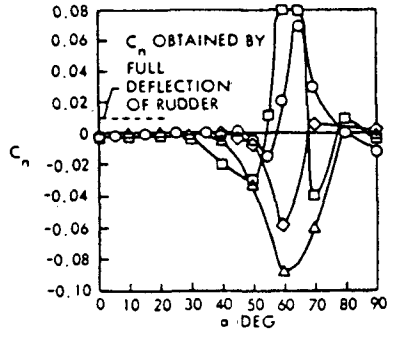

b. VARIATION OF STATIC YAWING-MOMENT COEFFICIENT WITH ANGLE-OF-ATTACK FOR SEVERAL MODELS OF THE CONFIGURATION

Figure 1. Typical High-Alpha Wind Tunnel Test Results

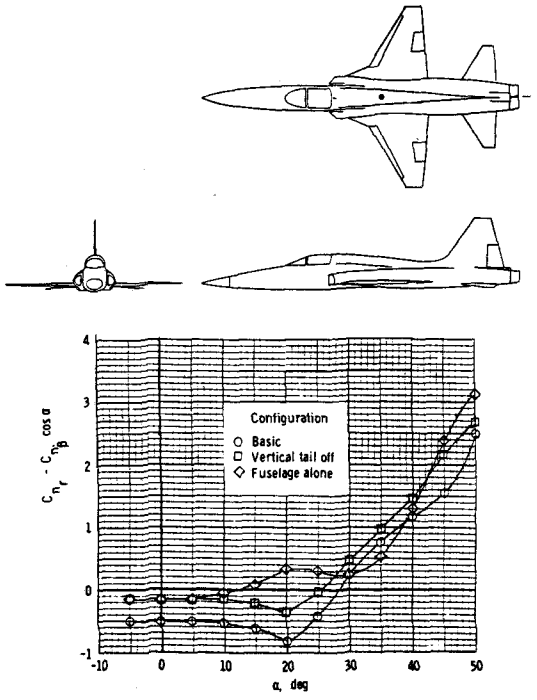

Figure 2. Aircraft Yaw Damping

II.1 Yaw Characteristics

Results such as those shown in Figure 2 justify the use in Reference 12 of the ogive-cylinder body-alone experimental results to represent the high-alpha lateral aerodynamics of advanced aircraft. Utilizing the fact that for an asymmetric body to every α, β combination there corresponds a specific σ , ϕ pair (where σ is the total angle of attack) the $C_y(\phi)$ characteristics shown in Figure 3 were used to derive the $C_y(\beta)$ characteristics in Figure 4. Locating the switch between the positive and negative $C_y(\phi)$ extremes in Figure 3, due to nose microasymmetry, at the ϕ value listed under ROLL DATUM in Figure 4, the crossover between the corresponding $C_y(\beta)$ extremes in Figure 4 could occur anywhere in the range $-30° < \beta < 30°$. Letting these ogive-cylinder side force data represent the slender forebody of an F-111 aircraft model, the envelopes for the $C_n(\beta)$ characteristics measured in a wind tunnel test[13] were well predicted (Figure 5). The fact that the transfer between the envelope-branches occurred near

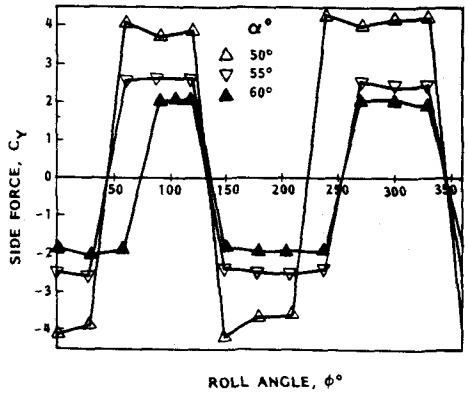

Figure 3. Side Force Characteristics of a 3.5d Ogive

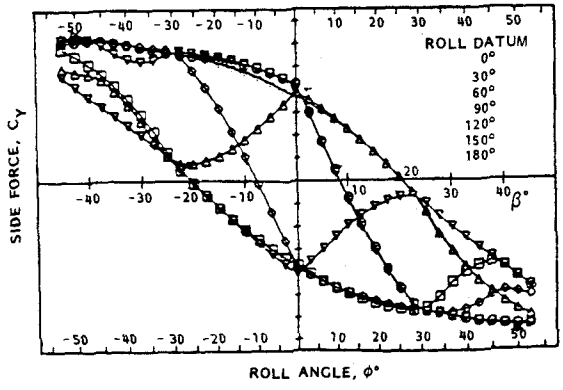

Figure 4. Multiple Solutions for $C_y(\beta)$ of a 3.5 d Ogive.

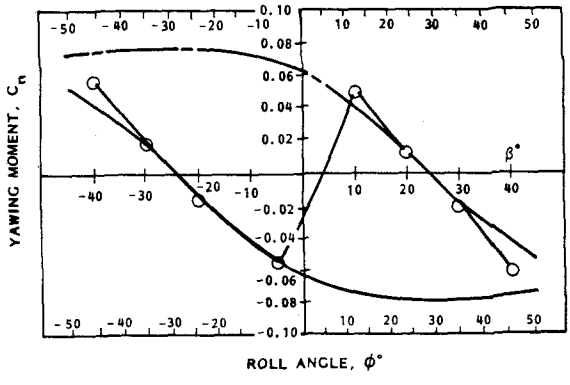

Figure 5. Yawing Moment $C_n/(\beta)$ for Model of the F-111 Aircraft

ß = O in the test was more or less accidental, as it could occur anywhere in the range -30° < ß < 30° (Figure 4).

Based upon this ϕ-ß correlation the characteristics shown in Figure 6 were presented in Reference 12 as equally possible forms of the $C_y(ß)$ and $C_n(ß)$ characteristics of advanced aircraft; and it was suggested that extensive static tests be performed to determine which of the different characteristics in Figure 6 applied to the advanced aircraft under consideration. Aside from the well known large effect of Reynolds number[14], which would severely limit the possibility of extropolating such subscale test results to full scale, the results in Figure 1 demonstrate that any one of the different characteristics in Figure 6 would be equally likely to occur in full-scale flight, presenting the pilot with quite a problem; a problem that fortunately never will materialize.

The full-scale vehicle in free flight will only enter the high-alpha flight regime when performing maneuvers, where the associated moving-wall effects[15] will over-power the (static) effects of nose microasymmetry. Even a very modest roll rate has been shown to have a large effect on the developed side force,[16] and the moving wall effect generated by a coning motion has been shown to be equally powerful[17] (Figure 7). Only a slight push was needed to establish the coning motion in one direction or the other, in spite of the fact that the static yawing moment at ß=O was biased in one direction due to nose micro-asymmetry. The cone-cylinder body reached equal steady-state coning rates in both directions (Figure 8). That is, the motion-induced moving wall effect, illustrated in Figure 9, dominated over the static asymmetry, locking-in the separation-asymmetry in the direction of the motion, driving it until the drag generated yawing moment balances the moment generated by the separation asymmetry[18] (Figure 10). (The prediction[18] neglects the bearing friction present in the test.)

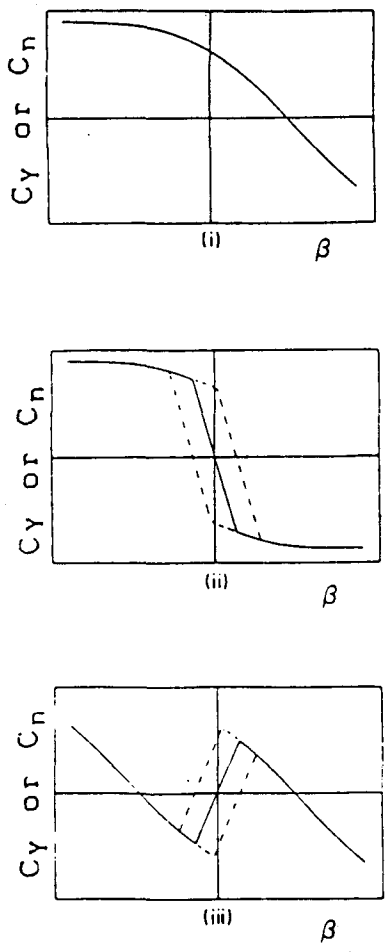

Figure 6. Possible Variations of $C_y(ß)$ and $C_n/ß)$ characteristics

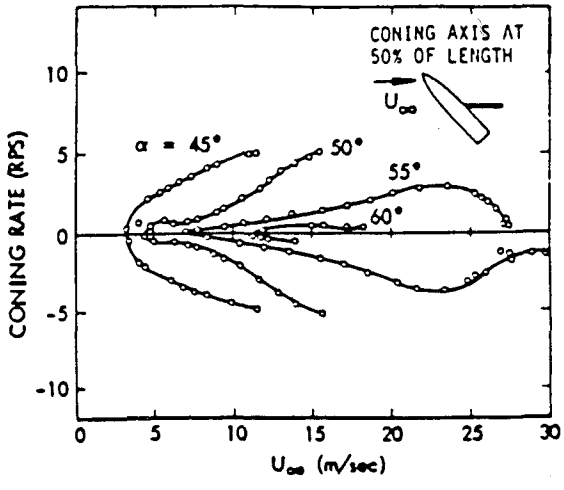

Figure 7. Dual Coning Characteristics of a Cone-Cylinder Model

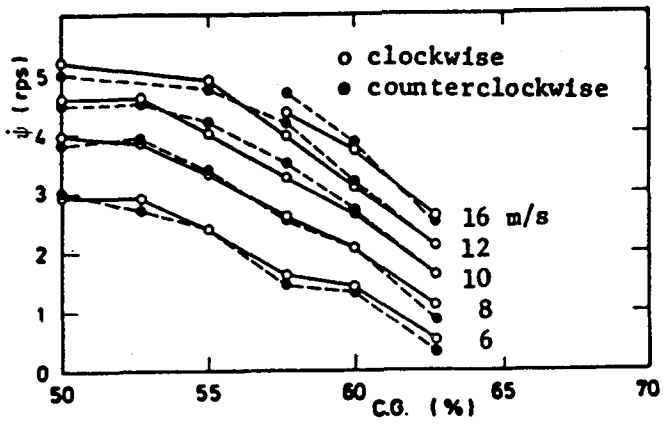

Figure 8. Steady State Coning Rate of Cone-Cylinder Model

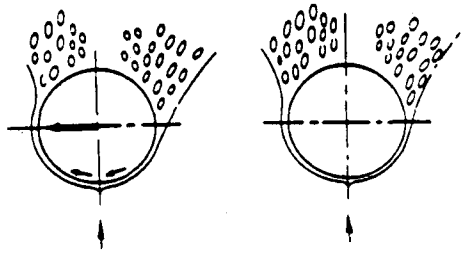

Figure 9. Moving Wall Effect on Translating Circular Cross-Section

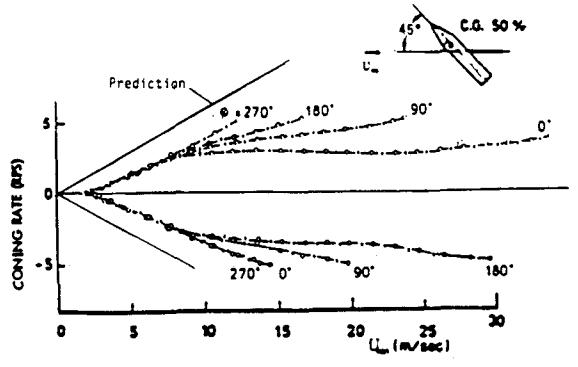

Figure 10. Coning Characteristics of Pointed Cone-Cylinder Body

The experimental results[17] in Figure 10 demonstrate that, during the initial "spin-up" of the coning motion, the effect of roll-angle, which is large in static tests at similar laminar test conditions (Figure 3), is completely overpowered by the moving wall effect. Consequently, on an advanced aircraft, performing a high-alpha maneuver at moderate side-slip angles, it is the moving-wall effect, realized in the boundary layer build-up region near the flow stagnation point on the nose, that will determine which way the nose side force, illustrated in Figure 3, will "flip".

II.1.1 Oscillatory Coning. When the cone-cylinder model was turned around 180 deg., the results shown in Figure 11 were obtained[17]. In this case the coning motion changed direction without any external forcing, "spinning up" to the limiting rates in both directions before slowing down and starting coning in the opposite direction. The fluid dynamics behind this behavior can be understood by studying Magnus lift results for a rotating circular cylinder[19] (Figure 12). At low rotation rates the downstream moving wall effect delays separation on the top side, generating greater suction. On the opposite side, the upstream moving wall effect promotes separation. This results in a positive lift that is proportional to the wall-to-freestream velocity ratio, U_W/U_∞. At some critical value of U_W/U_∞, transition of the laminar boundary layer to a turbulent layer occurs on the bottom side due to the upstream moving wall effect. As a consequence, the separation type changes to turbulent separation, while laminar separation

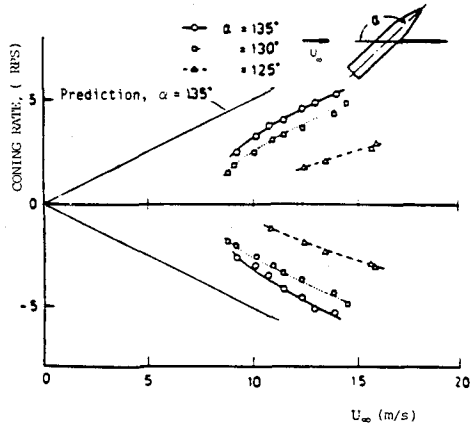

Figure 11. Coning Characteristics of Cone-Cylinder Model Flying Backwards

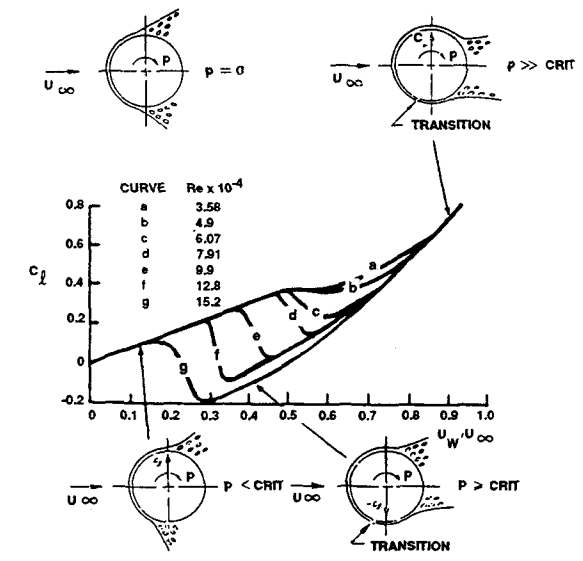

Figure 12. Magnus Lift Characteristics for Initially Laminar Flow Conditions

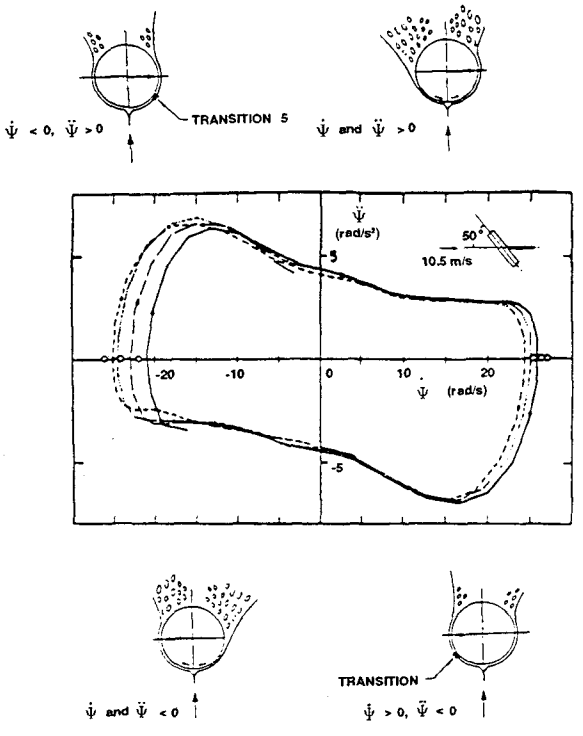

Figure 13. Reversal of Coning Motion for Flat-Faced Circular Cylinder

is maintained on the top side. This reverses the separation asymmetry, generating a negative Magnus lift.

A similar reversal of the separation asymmetry occurs for the coning body (Fig. 13). Initially, flow asymmetry and/or minute surface irregularities set the separation asymmetry. The ensuing coning motion reinforces the effects of the asymmetry, as the laminar separation is delayed or the advancing side and promoted on the retreating side, generating a force that drives the coning ($\dot\psi$ and $\ddot\psi$ < 0). However, the moving wall effect eventually causes boundary layer transition on the retreating side, reversing the separation asymmetry (i.e., $\dot\psi$ > 0 but $\ddot\psi$ < 0). Eventually this results in accelerated coning in the opposite direction ($\dot\psi$ and $\ddot\psi$ < 0). The rotation reversal moves transition back into the wake on the new advancing side, and asymmetric laminar separation is re-established. Eventually, transition occurs on the retreating side, reversing the separation asymmetry and decelerating the coning motion ($\dot\psi$ < 0 but $\ddot\psi$ > 0). The process repeats itself, resulting in a self-reversing, oscillatory coning motion. It will be seen in what follows that a similar process for the rolling body drives the wing-rock of slender-nosed aircraft.

II.2 Roll Characteristics

Smoke flow visulation revealed that the violent wing rock observed in wind tunnel tests of a generic aircraft configuration[19] (Figure 14) was probably generated by asymmetric vortex shedding from the slender forebody. As the Reynolds number was in the critical region, Re = 0.26 x 10^6, the Magnus reversal shown in Figure 12 will occur very close to U_W/U_∞ = 0. This suggests that the wing rock is generated by a forebody flow phenomenon similar to that causing oscillatory coning, with the moving wall effects generated by rolling rather than by coning. The following scenario can be visualized[20] (Figure 15). At t = t_1, the adverse upstream moving-wall effect on the forebody crossflow causes boundary layer

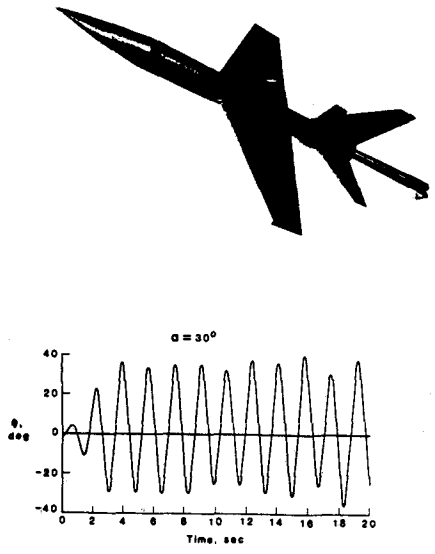

Figure 14. Wing Rock Buildup at α = 30 deg.

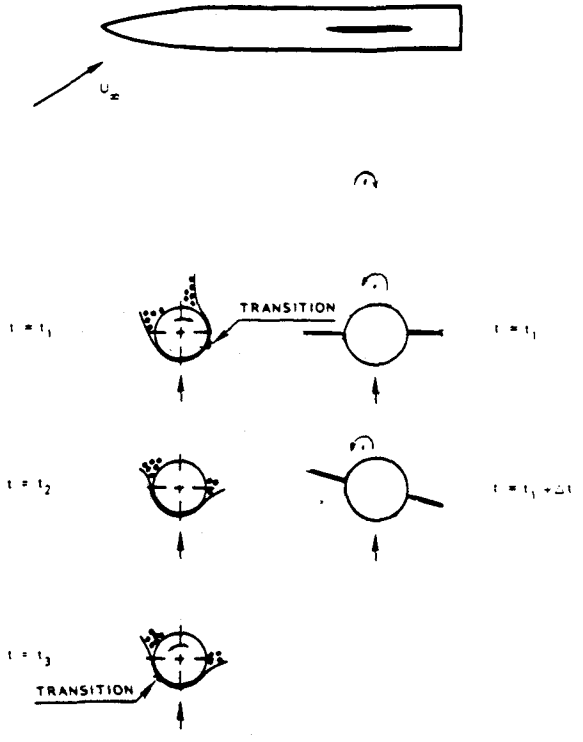

Figure 15. Conceptual Flow Mechanism for Nose-Induced Wing Rock

transition to occur earlier, switching the separation toward the supercritical type. In absence of any time lag, the vortex geometry sketched at t = t, would result. Due to convective time lag effects, similar to those generating slender wing rock[21], this vortex geometry is not realized until $t = t_2 = t_1 + \Delta t$. Only the lower vortex is shown as only it will induce significant loads on the wing-body geometry, generating portside downwash with associated statically stabilizing rolling moment. This produces the positive aerodynamic spring needed for the oscillatory wing rock motion. At $t = t_3$, when the roll rate reaches its maximum in the opposite direction, another switch in the forebody separation asymmetry occurs. Because of the convective time lag effect, the vortex geometry at the (now horizontal) wing has not changed, but is the same as at $t = t_2$, in agreement with flow visualization results.[19] During the time lag Δt, the vortex-induced rolling moment drives the rolling motion, generating the observed wing rock.[21]

When comparing the wing rock in Figure 14 with that observed on an 80 deg. delta wing[22] (Figure 16), one finds it to be much more violent, building up to the limit cycle amplitude, $\Delta\psi$ 35°, in less than 3 cycles compared to the more than 10 cycles needed in the case of the slender wing rock. It is described at length in Reference 23 how the extent, both circumferentially and axially of the critical separated flow region[24] (Figure 17) grows from half cycle to half cycle, and with it the

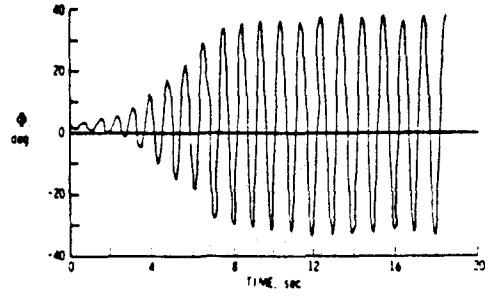

Figure 16. Wing Rock Buildup for an 80 deg. Delta Wing

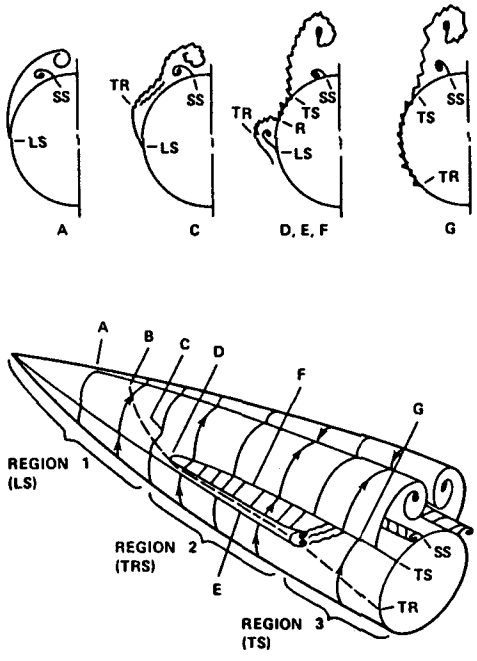

Figure 17. Flow Visualization Results for a Pointed 3.5d Ogive at M = 0.25 and α = 55 deg.

strength of the asymmetric vortices, generating a much faster amplitude build-up than in the case of slender wing rock[21] where the vortex stength remains constant (from half cycle to half cycle).

Figure 18 shows some of the wing-body geometries tested by Brandon, et al[19,25]. For the aft wing position, the interactive flow phenomenon remained the same, and there was only a moderate effect of the body cross-sectional shape (Figure 19a). For the forward wing position, however, the interactive flow mechanism changed dramatically with the cross-sectional shape, with associated large impact on the wing rock characteristics (Figure 19b). The three different types of flow interaction are describe at length in Reference 23.

III. PREDICTION METHODOLOGY

When considering the existing strong coupling between vehicle motion and complex flow phenomena, such as boundary layer transition and flow separation, discussed earlier, one can understand why there are no purely theoretical methods available for prediction of the unsteady

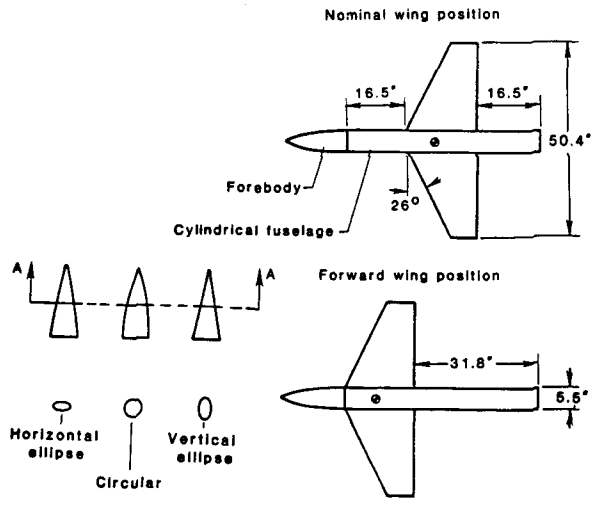

Figure 18. Tested Wing-Body Geometries

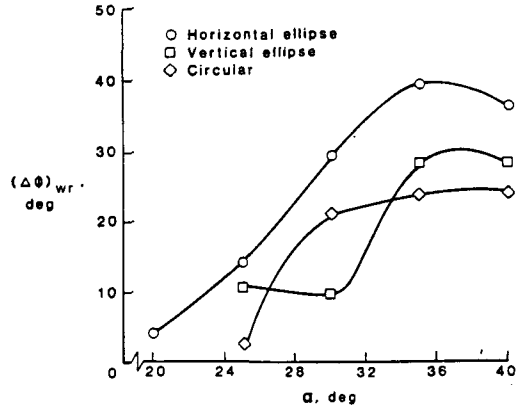

a. Nominal wing position

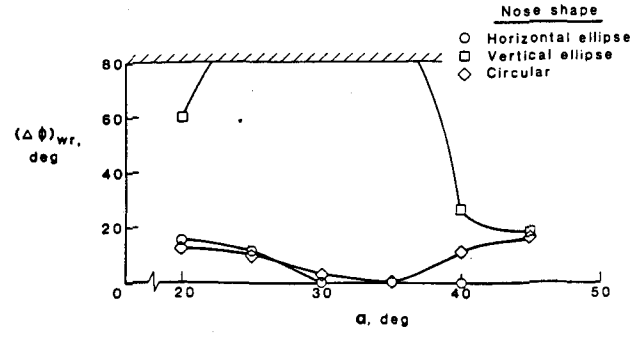

b. Forward wing position

Figure 19. Effect of Forebody Cross-Sectional Shape on Wing Rock Amplitude

aerodynamics of advanced aircraft or missiles operating at high angles of attack. The only manner in which a realistic prediction of high-alpha aerodynamics presently could be accomplished, short of full-scale flight investigation, is through semi-emperical means, i.e., by using experiment and theory together to provide dynamic simulation of full-scale vehicle dynamics through analytic extrapolation from subscale test data. This has been accomplished for planar motion of a number of vehicle geometries.[26,27] However, in the case of the high-alpha dynamics of advanced aircraft, the coning and rolling motions, with associated moving wall effects on flow separation and associated vortex shedding greatly complicate the problem of dynamic simulation in experiments and, even more so, the problem of prediction of the vehicle dynamics. A step-by-step approach is needed for development of the building blocks that can lead to a full predictive capability.

III.1 Coning Motion

The developed method for prediction of slender-body coning characteristics[18] has limited application by itself. This is true even for laminar flow in the case of incipient asymmetric flow conditions. Another limitation is that only one cell of asymmetric flow separation is allowed. The most severe limitation is, of course, that the method cannot be applied to flow conditions that are not laminar, such as will usually be the case for the full-scale vehicle. Methods will have to be developed for computation of the transition effect on high-alpha aerodynamics before prediction of full-scale coning and/or nose slice of aircraft and missiles will be possible. Until such time, the only recourse available is to compute the maximum possible yawing moment due to forebody separation asymmetry, using the means described in Reference 14. In most cases the yawing moment predicted in this manner will probably exceed the available control capability, and some form of control of the forebody flow asymmetry[28] will be needed.

III.2 Wing Rock

In the case of wing rock generated by forebody vortices, further research is needed to establish the asymmetric vortex characteristics generated by a certain forebody separation asymmetry; including the maximum possible one generating the maximum yawing moment discussed earlier. It should also be noted that at full-scale Reynolds numbers the critical flow region (see Figure 17) will be located close to the apex and one would, therefore, expect the wing rock to be much less violent than the one observed in a test at conditions close to those giving the maximum wing rock amplitude[19,20] (Figure 14). Test results for the X-29A aircraft indicate such very strong effect of Reynolds number.[29] Whereas both subscale wind tunnel tests and the drop test of a 22% model of X-29A showed wing rock due to dynamic wing stall[30] to occur (Fig. 20), in spite of a large difference in Reynolds number, the forebody-induced wing rock that occurred at higher angles of attack on the drop model, when the stall-induced wing rock had been eliminated by use of aileron-supplied roll damping (Figure 21)*, apparently was not of significant magnitude at full-scale Reynolds number to present the pilot with any problem.[31] As could be expected,[7,32] the increase in

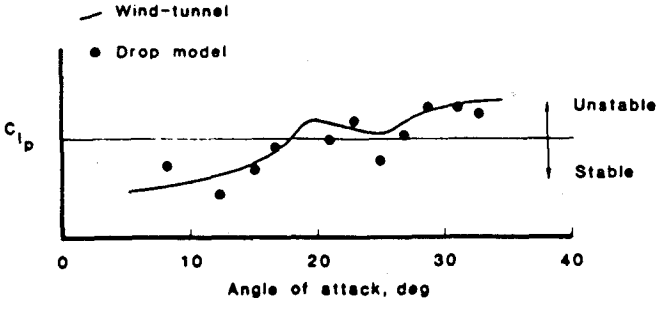

Figure 20. Roll Damping of X-29A Models

*Courtesy of the authors of Reference 29. This figure was shown in the oral presentation at the AIAA Atmospheric Flight Mechanics Conference, Monterey, California, Aug. 17-29, 1987, but is not contained in Reference 29.

Reynolds number decreased the dynamic stall effect and ... "only mild wing rock was encountered up to 35 deg., but it diminished at 45 deg. to the point that 'wing rock is not a factor', Smith (the pilot) said." "So far, the airplane has (performed) significantly better than predicted", he said.

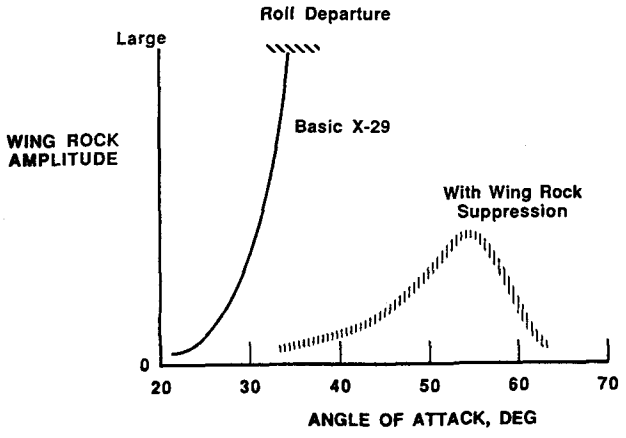

Figure 21. Wing Rock Characteristics of the X-29 Aircraft

Going back to Figure 13 one can see that the coupling between vehicle motion and boundary layer transition, which drives the forebody-induced high-alpha wing rock, will have a damping effect on coning or nose-slice motions. This can explain the agreement in Figure 20 between test results obtained in one (roll) degree-of-freedom wind tunnel tests and free flight results for a 22% scale model. However, at full-scale Reynolds number, when the critical flow region (Figure 17) was "squished" to a small region near apex and because of insignificant size to drive the high-alpha wing rock, the damping effect on the coning motion was, of course, lost also. This may explain the fact that in full-scale flight ".... at 45 deg. AOA leaving the control stick centered allowed a nose-right, 8 deg./sec. yaw rate to develop."[31]

IV. CONCLUSIONS

Analysis of the problems associated with the prediction of high-alpha vehicle dynamics reveals the following:

1. Most important is the requirement of a thorough understanding of the flow phenomena dominating the high-alpha unsteady aerodynamics.

2. Acquiring some degree of quantitative predictive capability of the various unsteady flow modules comprising the high-alpha vehicle dynamics will greatly enhance once capability to design an aircraft or missile with the desired agility.

3. The first milestone towards the achievement of full predictive capability is the development of means for analytic extrapolation from subscale test data to full-scale flight conditions.

V. REFERENCES

1. Many authors, "Dynamic Stability Parameters", AGARD CP-235, Nov. 1978.

2. Ericsson, L. E., "Technical Evaluation Report on the Fluid Dynamics Panel Symposium on Dynamic Stability Parameters", AGARD-AR-137, April 1978.

3. Ericsson, L. E., "A Summary of AGARD FDP Meeting on Dynamic Stability Parameters", Paper 2, AGARD CP-260, May 1979.

4. Orlik-Ruckemann, K. J., "Dynamic Stability Testing of Aircraft--Needs Versus Capabilities", Progress Aerospace Sci., Pergamon Press. 1975.

5. Ericsson, L. E., and Reding, J. P., "Review of Support Interference in Dynamic Tests" AIAA Journal, Vol. 21, No. 12, Dec. 1983, pp. 1652-1666.

6. Ericsson, L. E., and Reding, J.P., Dynamic Support Interference in High Alpha Testing," Journal of Aircraft, Vol. 23, Dec. 1986, pp. 889-896.

7. Ericsson, L. E., and Reding, J. P., "Scaling Problems in Dynamic Tests of Aircraft-Like Configurations", Paper 25, AGARD CP-227, Sept. 26-28, 1977.

8. Ericsson, L. E., "Reflections Regarding Recent Rotary Rig Results", Journal of Aircraft, Vol. 24, Jan. 1987, pp. 25-30

9. McElroy, G.E. and Sharp, P.S., "An Approach to Stall/Spin Development and Test", AIAA Paper No. 71-772, July 1971.

10. Malcolm, G. N., Ng, T. T., Lewis, L. C., and Murri, D.G., "Development of Non-Conventional Control Methods for High Angle of Attack Flight Using Vortex Manipulation", AIAA Paper 89-2192-CP, Aug. 1989.

11. Grafton, S. B., Chambers, J. R., and Coe, Jr., P. L., "Wind-Tunnel Free-Flight Investigation of a Model of a Spin Resistant Fighter Configuration", NASA TN D-7716, June 1974.

12. Lamont, P. and Kennaugh, A., "Multiple Solutions for Aircraft Sideslip Behavior at High Angles of Attack", AIAA Paper 89-0645, Jan. 1989.

13. Chambers, J. R., Anglin, E. L., and Bowman, Jr., J. S., "Effects of a Pointed Nose on Spin Characteristics of a Fighter Airplane Model Including Correlation with Theoretical Calculations", NASA TN D-5921 (1970).

14. Ericsson, L. E. and Reding, J.P., "Asymmetric Vortex Shedding from Bodies of Revolution", Chapter VII, Tactical Missile Aerodynamics, Vol. 104, Progress Astro and Aero. Series, M. J., Hemsch and J. N. Nielson editors, (1986), pp 243-296.

15. Ericsson, L. E., "Moving Wall Effects in Unsteady Flow", Journal of Aircraft, Vol. 25, Nov. 1988, pp. 977-990.

16. Atraghji, E. G., "The Influence of Mach Number, Semi-Nose Angle and Roll Rate on the Development of the Forces and Moments Over a Series of Long Slender Bodies of Revolution at Incidence" NAE Data Report 5x5/0020, (1967), National Research Council, Ottawa, Canada.

17. Yoshinaga, T., Tate, A., and Inoue, K., "Coning Motion of Slender Bodies at High Angles of Attack in Low Speed Flow", AIAA Paper 81-1899, Aug. 1981.

18. Ericsson, L. E., "Prediction of Slender Body Coning Characteristics', AIAA Paper No. 89-2223, Aug. 1989.

19. Brandon, J. M. and Nguyen, L. T., "Experimental Study of Effects of Forebody Geometry on High Angle of Attack Static and Dynamic Stability", AIAA Paper 86-0331, Jan. 1986.

20. Ericsson, L. E., "Wing Rock Generated by Forebody Vortics", J. Aircraft, Vol. 26, Feb. 1989, pp 110-116.

21. Ericsson, L. E., "The Fluid Mechanics of Slender Wing Rock", J. Aircarft, Vol. 21, May 1984, pp 322-328.

22. Nguyen, L., Yip, L. and Chambers, J., "Self-Induced Wing Rock of Slender Delta Wings", AIAA Paper 81-1883, Aug. 1981.

23. Ericsson, L. E., "Further Analysis of Wing Rock Generated by Forebody Vortices", J. Aircraft, Vol. 26, Dec. 1989, pp 1098-1104.

24. Keener, E. R., "Flow-Separation Patterns on Symmetric Forebodies", NASA TM 86016, Jan. 1986.

25. Brandon, J. M., Murri, D. G. and Nguyen, L. T., "Experimental Study of Effects of Forebody Geometry on High Angle of Attack Static and Dynamic Stability and Control", ICAS Paper 86-5.4.1, Sept. 1986.

26. Ericsson, L. E. and Reding, J. P., "Dynamic Simulation Through Analytic Extrapolation", J. Spacecraft and Rockets, Vol. 9, March - April 1982, pp. 160-166.

27. Ericsson, L. E. and Reding, J. P., "Analytic Extrapolation to Fullscale Aircraft Dynamics", J. Aircraft, Vol. 21, March 1984, pp 222-224.

28. Ericsson, L. E., "Control of Forebody Flow Asymmetry, a Critical Review", AIAA Paper No. 90-2833, Aug. 1990.

29. Fratello, D. J., Croom, M. A. Nguyen, L. T., and Domack, C. S., "Use of the Updated NASA Langley Radio-Controlled Drop-Model Technique for High-Alpha Studies of the X-29A Configuration", AIAA Paper 87-2559, Aug. 1987.

30. Ericsson, L. E., "The Various Sources of Wing Rock", AIAA Paper 88-4370, Aug. 1988.

31. Scott, W. B., "High AOA Characteristics of X-29 Exceed Predictions", Aviation Week & Space Technology, March 5, 1990, pp 68-69.

32. Ericsson, L. E. and Reding, J. P. "Fluid Mechanics of Dynamic Stall, Part II, Prediction of Full Scale Characteristics", J. Fluids and Structures, Vol. 2, March 1988, pp 113-143.